Highly Efficient Inverted Type-I CdS/CdSe Core/Shell Structure QD-Sensitized Solar Cells

Zhenxiao Pan, Hua Zhang, Kan Cheng, Yumei Hou, Jianli Hua, and Xinhua Zhong*

Shanghai Key Laboratory of Functional Materials Chemistry, Institute of Applied Chemistry, East China University of Science and Technology, Shanghai 200237, China

ABSTRACT

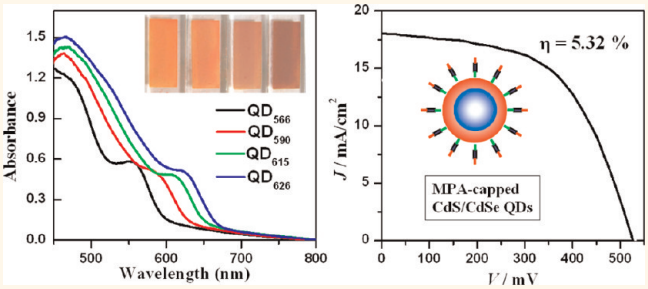

Presynthesized high-quality CdS/CdSe inverted type-I core/shell structure QDs have been deposited onto TiO_2 electrodes after first coating with bifunctional linker molecules, mercaptopropionic acid (MPA), and the resulting quantum dot sensitized solar cells (QDSCs) exhibited record conversion efficiency of 5.32% (V_{oc} = 0.527 V, J_{sc} = 18.02 mA/cm^2, FF = 0.56) under simulated AM 1.5, 100 mW cm^{-2} illumination. CdS/CdSe QDs with different CdSe shell thicknesses and different corresponding absorption onsets were prepared *via* the well-developed organometallic high-temperature injection method. MPA-capped water-dispersible QDs were then obtained *via* ligand exchange from the initial organic ligand capped oil-dispersible QDs. The QD-sensitized TiO_2 electrodes were facilely prepared by pipetting the MPA-capped CdS/CdSe QD aqueous solution onto the TiO_2 film, followed by a covering process with a ZnS layer and a postsintering process at 300 °C. Polysulfide electrolyte and Cu_2S counterelectrode were used to provide higher photocurrents and fill factors of the constructed cell devices. The characteristics of these QDSCs were studied in more detail by optical measurements, incidental photo-to-current efficiency measurements, and impedance spectroscopy. With the combination of the modified deposition technique with use of linker molecule MPA-capped water-soluble QDs and well-developed inverted type-I core/shell structure of the sensitizer together with the sintering treatment of QD-bound TiO_2 electrodes, the resulting CdS/CdSe-sensitized solar cells show a record photovoltaic performance with a conversion efficiency of 5.32%.

KEYWORDS: quantum dot sensitized solar cells · core/shell structure · CdS/CdSe · high conversion efficiency · sintering treatment

Great effort has been focused on efficiently exploiting solar energy to meet energy and environmental demands.[1] Quantum dot sensitized solar cells (QDSCs) constitute one of the most promising low-cost candidates for third-generation photovoltaic cells due to the potential advantages of multiexciton generation and the extraction of nonthermalized charge carrier.[2−9] Theoretically, the maximum thermodynamic conversion efficiency (η) of a QDSC can reach 44%.[9] Although QDSCs have been studied for many years, at present the reported best η values for liquid junction QDSCs are typically below 5%,[10−16] and for solid-state QDSCs they are in the range 5−6.18%,[17,18] partially because of unsatisfactory coverage of QDs on the TiO_2 electrodes and the limitation of adsorption range of QD sensitizers.[19−21]

Pursuing higher conversion efficiency is always a core task for solar cells, and one of the current key issues is to search for suitable panchromatic sensitizers to enhance the harvest of solar light. Although the utilization of QDs with large size or narrow band gap can expand the light harvest range, electron-injecting efficiency was sacrificed due to the lower conduction band edge. Among the wide variety of QDs used as sensitizers in QDSCs (such as PbS,[22,23] InP,[24] Bi_2S_3,[25] CdTe,[26] CdS,[27−29] CdSe[30−34]), CdS and CdSe are promising materials reported to have better performance. Comparing between the two materials, CdS QD-based cell devices have a higher open-circuit voltage; however, the high band gap of CdS (2.25 eV in bulk) limits its absorption range below *ca.* 550 nm. In contrast, although the absorption range of CdSe can extend to *ca.*720 nm, the electron injection efficiency of CdSe QD-based solar cells is less than that of CdS-based ones. It is meaningful to explore QDs with a wide adsorption range and high electron-injecting efficiency simultaneously. To combine both advantages of the CdS and CdSe materials in light harvesting and electron injection, in recent years, novel inverted type-I CdS/CdSe core/shell structure QD-based solar cells have received considerable interest for their special photoelectronic features.[14−16,35−41] In this so-called inverted type-I core/shell structure, where a material with narrower band gap is grown

* Address correspondence to zhongxh@ecust.edu.cn.

Received for review January 18, 2012 and accepted April 18, 2012.

Published online April 18, 2012
10.1021/nn300278z

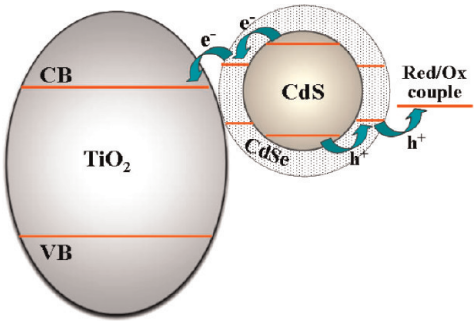

Figure 1. Schematic illustration of band edge alignment of the inverted type-I CdS/CdSe core/shell structure QD-sensitized solar cells.

expitaxially around the core material with a higher band gap, the charge carriers (electron and hole) are distributed largely in the shell region.[42] This favors the extraction of photogenerated electrons and enhances the electron injection rate accordingly.[35] Meanwhile, the redistribution of the electrons in the CdS/CdSe core/shell structure is supposed to trigger a downward and upward shift of the band edges. Therefore, the resulting band edges for CdS/CdSe-sensitized TiO_2 photoelectrodes are inferred to have a cascade structure, as shown in Figure 1. The conduction band levels of the three materials decrease in the order CdSe > CdS > TiO_2. That is, the inverted type-I CdS/CdSe core/shell structure QDs give a higher driving force for injection of excited electrons out of the QD sensitizers in comparison with plain CdSe QDs. This facilitates the transfer of electrons from QD sensitizer to TiO_2 substrate, resulting in improved electron-injection efficiency and photovoltaic performance in the corresponding cell devices. It should be noted that almost all CdS/CdSe-sensitized solar cells reported previously were prepared with the use of direct growth of QDs onto TiO_2 film electrodes *via* chemical bath deposition or by successive ionic layer adsorption and reaction (SILAR).[14−16,36−41] Although this direct growth route can ensure high coverage of QDs, precise control of particle size, size distribution, and especially the exact inverted type-I core/shell structure cannot be achieved due to the uncontrollability of nucleation and growth of the QDs on the mesoporous TiO_2 surfaces.[9,19] Accordingly, the resulting CdS/CdSe-sensitized QDSCs prepared by this direct growth route could not obtain a satisfied efficiency.

Use of previously prepared QDs can avoid the drawbacks of the direct growth method; however, it is still a great challenge to immobilize the previously prepared QDs onto TiO_2 electrodes with high surface coverage and achieve good photovoltaic performance of the resulting cell devices. The main route for immobilization of presynthesized QDs to the TiO_2 film electrodes is achieved by functionalization of the TiO_2 substrate with bifunctional linker molecules (typically mercaptoalkaboic acids), followed by attachment of the initial oil-soluble QDs to the adsorbed linkers.[30−33,35,44−46] This deposition method has been plagued by low and irreproducible surface coverage of QDs, and the η values of the resulting QDSCs are typically in the range 1−2%, which are remarkably less than the corresponding cell devices prepared by the direct growth method. Herein, we took advantage of the tremendous development in organometallic high-temperature synthesis methods for the preparation of high-quality inverted type-I CdS/CdSe core/shell structure QDs and assembled the presynthesized colloidal QDs to the TiO_2 electrodes with the use of bifunctional linker molecule, mercaptopropionic acid (MPA), capped water-soluble QDs. The water-soluble MPA-capped CdS/CdSe QDs are obtained *via* the ligand exchange of the initial organic capping ligand by MPA. With the combination of the effective deposition technique and well-developed inverted type-I core/shell structure of the sensitizer together with the sintering treatment of the photoanodes, the resulting CdS/CdSe-based solar cells exhibit a high short-circuit current of 18.02 mA cm^{-2} and conversion efficiency of 5.32% under full 1 sun illumination. To our knowledge, this result is one of the best performances of liquid junction QDSCs.

RESULTS AND DISCUSSION

Inverted Type-I Core/Shell Structure QDs. Relying on the well-developed organometallic high-temperature synthetic methods, nearly monodispersed 2.9 nm CdS core QDs with absorption onset of 380 nm were first prepared in oleylamine media at high temperature;[47] then CdSe shells were grown over the CdS core template with the addition of the Cd/Se precursor to the crude CdS reactive solution.[42] The detailed procedure for the preparation of CdS and CdS/CdSe core/shell QDs is given in the Materials and Methods section. With the addition of the Cd/Se precursor to the crude CdS reactive solution, the enhancement of particle size as observed by TEM measurement (Figure 2) give direct evidence for the overgrowth of CdSe around the CdS core. Both the as-prepared core and core/shell structure QDs show a nearly spherical shape with a narrow size distribution of 4−6% relative standard deviation without any postpreparation fractionation or size sorting. With the increase of the CdSe shell thickness around the CdS cores, both the absorption onset in the absorption spectra and the band-edge photoluminescence (PL) emission peaks in the PL spectra shift systematically to the long-wavelength side (Figure 3). Both the single PL emission peak in the PL spectra and no CdSe-correlated absorption peak in the absorption spectra can confirm the formation of a core/shell structure and rule out any separate homogeneous nucleation of CdSe nanocrystals. Details on the characterization of the core/shell structure are described elsewhere.[42,48] For the plain CdS QDs, only a trap emission was observed with a broad peak

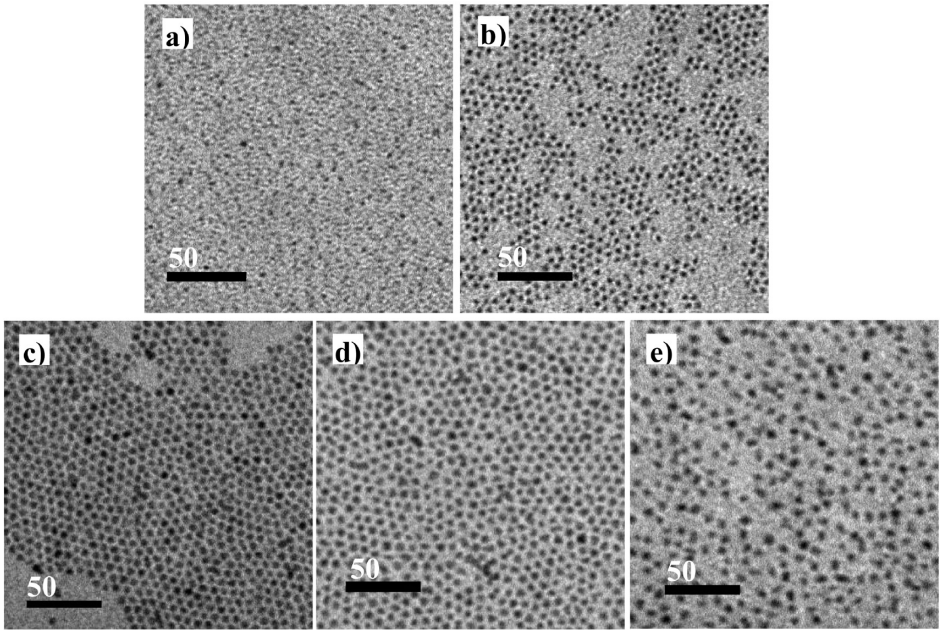

Figure 2. TEM images of 2.9 nm CdS cores (a) and derivate CdS/CdSe core/shell structure QDs with sizes of 4.6, 5.7, 6.1, and 6.7 nm (b–e). Their corresponding absorption and PL emission spectra are shown in Figure 3.

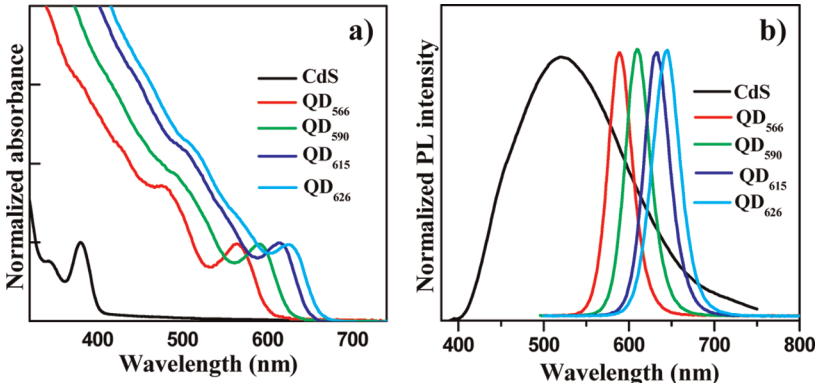

Figure 3. Absorption (a) and PL spectra (b, λ_{ex} = 350 nm) of CdS and derivate CdS/CdSe core/shell QDs with different absorption onsets.

centered around 520 nm, and no band edge emission was observed. The obtained CdS/CdSe core/shell QDs gave a symmetric and narrow PL peak. The small Stökes shift (~15–25 nm) between the emission peaks and the corresponding first excitonic absorption onsets indicates the dominant band edge luminescence from the core/shell nanocrystals without the appearance of deep trap emission at the long-wavelength side. It is noted that the absence of trap emission is favorable for high photocurrent in the final cell devices due to the decrease of electron recombination.[2–4,49] All the core/shell QD samples exhibit a low PL emission efficiency at the level of 1–5%. In the absorption spectra, all samples show a sharp first excitonic absorption onset. Such a distinct absorption feature cannot be achieved in the former cases prepared *via* the direct growth route.[14–16,36–41] With the increase of CdSe shell thickness, on one hand, the absorption onset is extended to wavelengths of λ = 566, 590, 615, 626 nm (for simplicity, hereafter denoted as QD_{566}, QD_{590}, QD_{615}, and QD_{626}, respectively); on the other hand, the absorptivity at the short-wavelength side (*i.e.*, wavelengths shorter than the absorption onset) is enhanced steadily. These absorption features demonstrate that with the formation of CdS/CdSe core/shell structure, the narrow absorption range of CdS QDs is expanded remarkably to the long wavelength and the light harvest efficiency is enhanced remarkably. Undoubtedly, this observed wide absorption range is favorable for harvesting solar light in the cell devices.[3,4]

Deposition of CdS/CdSe QDs onto TiO_2 Electrodes. Even though the organometallic synthetic method can support high-quality CdS/CdSe core/shell QDs, it is still a great challenge to assemble previously prepared QDs onto TiO_2 electrodes with high surface coverage and achieve good photovoltaic performance of the

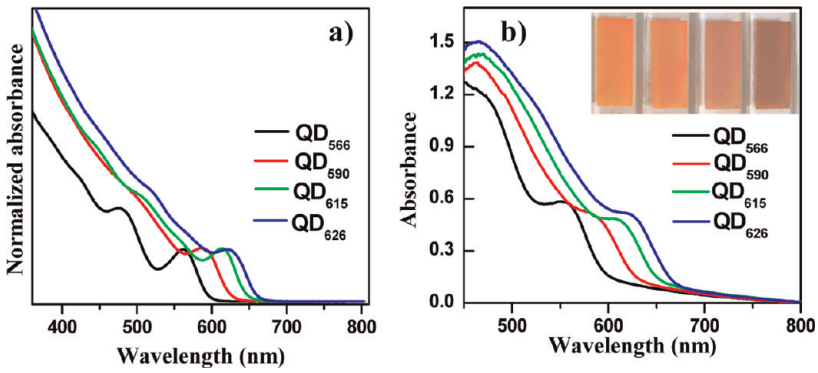

Figure 4. Adsorption spectra of MPA-capped water-soluble CdS/CdSe QDs with different absorption onsets (a) and the corresponding QDs anchored on 4 μm thick TiO_2 films (b). Inset: Photographs of these films presented in turn.

resulting cell device.[19−21,50] To improve the loading amount of the preprepared QDs onto TiO_2 electrodes, a modified deposition method with the use of bifunctional linker molecule MPA-capped water-soluble QDs was adopted. Four representative CdS/CdSe core/shell structure QDs (QD_{566}, QD_{590}, QD_{615}, and QD_{626}) were selected as sensitizer for the fabrication of solar cells. The initial oil-soluble QDs were transferred into water-soluble ones *via* ligand exchange with use of bifunctional MPA molecules. There was no distinguishable variation in the absorption spectra of the QDs before and after ligand exchange, as shown in Figures 3a and 4a, respectively, while the PL was quenched almost completely in the process of ligand exchange. The phenomena of PL quenching is commonly observed in plain CdSe QDs since the MPA molecules are known to act as a hole scavenger when attached to the CdSe QD surface.[51] Then the MPA-capped water-soluble QDs were deposited on mesoporous TiO_2 film by pipetting the MPA-capped QD aqueous solution (with absorbance of 2.0 at first absorption onset) onto the oxide matrix as described in the Materials and Methods section. The terminal carboxylate groups of MPA can bind QDs directly to TiO_2 surfaces. This is analogous to the case of carboxylate-terminated organic dye molecule binding to TiO_2, as adopted commonly in DSCs.[52]

The deposition of MPA-capped water-soluble QDs onto a TiO_2 electrode was very fast, and the first excitonic peak can approach the saturation absorbance value of ~0.6 in a period of 2 h. The successive deposition of presynthesized water-soluble colloidal CdSe QDs over mesoporous TiO_2 was accompanied by deepening of the color visible to the naked eye, as shown in the inset of Figure 4b. It should be noted that overextending the deposition time (more than 3 h) does not further increase QD loading, but brings forward a slight red-shift of the excitonic peak by about 2−3 nm, indicating the aggregation or interaction of the bond QDs. This would deteriorate the photovoltaic performance.[20] Figure 4b shows the absorption spectra of four representative CdS/CdSe QD-sensitized TiO_2 electrodes, and the corresponding MPA-capped QD aqueous solutions are also shown in Figure 4a for reference. Note that these spectra were recorded in the transmission mode using blank FTO/TiO_2 film as a reference. It was found that the spectral profiles and the sharp excitonic features of the colloidal QDs aqueous solutions were preserved after deposition onto the TiO_2 film, reflecting an unchanged particle size and nearly monodispersed size distribution. These features cannot be achieved by the direct growth of QDs onto TiO_2 film as reported in the literature.[14−16,36−41] The relatively high absorption of the visible light (absorbance >0.6) by these electrodes gives us intuitive information on high QD loading, which can also be visualized from the deep coloration of the electrodes in the inset of Figure 4b. The high absorbance ensures more than 85% of the incident light at wavelengths below the onset can be absorbed by the electrodes. The photograph of the electrodes shows the color that reflects their corresponding absorption spectra. Since the absorption spectrum of QD_{626} covers almost the whole visible spectrum, the QD_{626}-bound electrode shows a blackish color. Our success in achieving a relatively high loading amount of CdS/CdSe QDs in these TiO_2 films highlights the possibility of small-sized CdS/CdSe QDs penetrating the porous network of each TiO_2 film and thus providing a uniform coverage throughout the film. The uniformity of deposit of QDs along the TiO_2 thickness is verified by the observation that the absorbance of the QD-sensitized film is in linear relationship with the thickness of film (Figure S1 in the Supporting Information).

Transmission electronic microscopy (TEM) images give direct evidence to estimate the coverage of QDs over the TiO_2 film electrodes. With the aim of imaging the QD sensitizer on the TiO_2 surface directly, we deposited the QDs on the TiO_2 film electrodes without a scattering layer. After deposition, the films were scratched off the FTO glass and then dispersed in ethanol and dropped onto the TEM grid for TEM observation. In the control experiment, plain TiO_2 film without the deposition of QDs was also prepared and

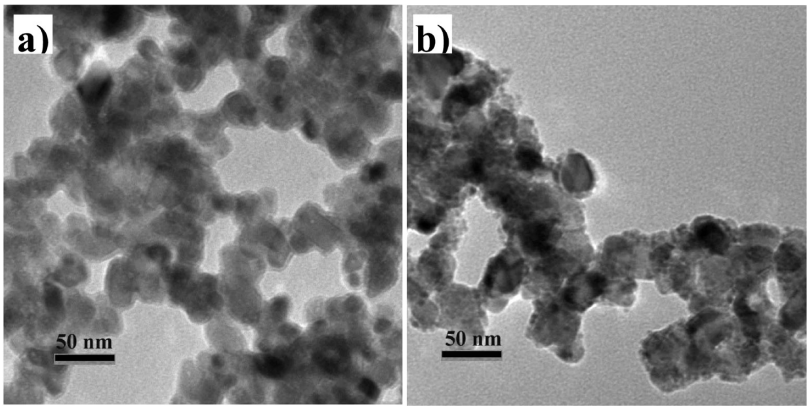

Figure 5. TEM images of plain TiO_2 film (a) and the CdS/CdSe QD-bound TiO_2 film (b).

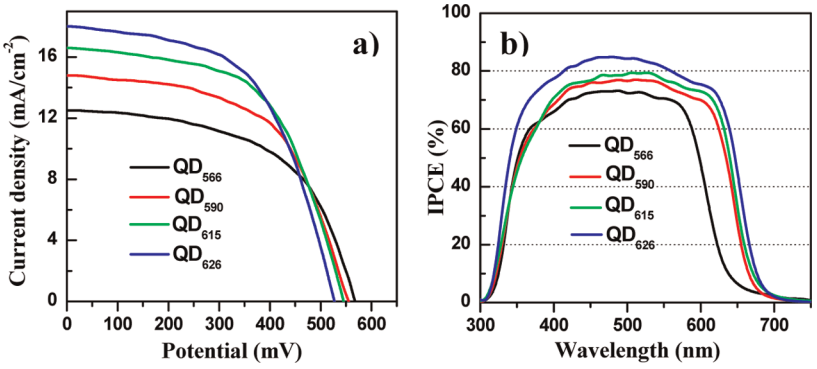

Figure 6. *J*–*V* curves (a) and IPCE spectra (b) of QDSCs based on CdS/CdSe QD sensitizers.

shown for comparison. The image of plain TiO_2 film (Figure 5a) shows well-connected TiO_2 nanoparticles and their clean bare surfaces with an average particle size of around 20–30 nm as reported by a commercial source. Figure 5b shows the image of a QD_{626}-bound TiO_2 film. From the image, the TiO_2 nanoparticle appears to be covered densely by smaller dots (CdS/CdSe QDs), which are more clearly seen at the edge side of the TiO_2 nanoparticles. The dense coverage of QDs over the TiO_2 film is in accordance with the high absorbance as observed in the absorption spectra.

It should be noted that this modified deposition method with use of linker-capped water-soluble QDs has been adopted in previous reports,[53–55] but the photovoltaic performance of the resulting cell devices is not improved in comparison with those through the commonly adopted postsynthesis assembly method with use of initial oil-soluble QDs, not to mention those by a direct growth method. The high QD loading in our case can be ascribed to the access of the highly stable linker MPA-capped QD aqueous solution. It was reported that stable water or methanol stock solutions of suspended MPA-QDs were unsuccessful due to the presence of residual organic ligands on the QD surface.[21] The nature of the initial hydrophobic ligand determines the degree of replacement by hydrophilic MPA in the ligand exchange process. In our work, the initial oil-soluble CdS/CdSe QDs were capped by oleylamine, which is a weaker capping reagent in comparison with the commonly used alkylphosphine oxide, alkylcarboxylic acid, or alkylphosphonic acid ligands. The weaker capping capacity of amines ensures the replacement by linker MPA molecules more completely. This favors the stability of MPA-QD aqueous dispersion and promotes the anchoring of QDs to TiO_2 electrodes. These features ensure the success of our adopted MPA-capped QDs deposited onto TiO_2 film. Furthermore, in comparison with the literature-adopted alcohol media,[54,55] our alkaline aqueous media favors the stabilization of MPA-QD dispersions due to the electrostatic repulsion effect.

Solar Cell Performance. After deposition of CdS/CdSe QDs, a thin passivation layer of ZnS was deposited onto the sensitized electrode by two SILAR deposition cycles, as done in most cell devices, followed by sintering in a muffle-type oven with a temperature of 300 °C for 2.5 min under an air atmosphere (the optimization processes for sintering temperature and sintering time are described in the following section). Sandwich-type thin layer cells were fabricated using the sintered FTO/TiO_2/QDs as the photoanode, Cu_2S on brass as the cathode, and a polysulfide electrolyte as the hole transporter. The *J*–*V* curves corresponding to solar cells sensitized by CdS/CdSe QDs with different

absorption onsets under an illumination of a solar simulator (AM 1.5 G) at 100 mW cm^{-2} are shown in Figure 6a, and the main photovoltaic parameters are listed in Table 1. For the tested cell devices, with the red-shift of absorption onset of QDs sensitizers from 566 to 626 nm, the open-circuit voltage (V_{oc}) decreased systematically from 568 to 527 mV, while the short-circuit current density (J_{sc}) increased substantially from 12.51 to 18.02 mA/cm^2. The systematical increase of J_{sc} is attributed to extending the light absorption range and the increase in absorptivity with red-shift of the absorption onset of QD sensitizers, as shown in Figure 4b. The QDSCs using QD_{626} as sensitizer exhibit the best performance, with J_{sc} = 18.02 mA/cm^2, V_{oc} = 0.527 V, fill factor (FF) = 0.56, and η = 5.32% under simulated AM 1.5 G, 100 mW cm^{-2} illumination. The obtained 5.32% conversion efficiency is believed to be one of the highest values in the liquid junction QDSCs so far. It is meaningful to note that higher photocurrent and conversion efficiency can be possibly achieved when CdS/CdSe QD sensitizers of longer wavelength absorption onsets are prepared with modification of the QD synthesis method.

TABLE 1. Photovoltaic Characteristics of QDSCs Based on Different QD sensitizers

QD	J_{sc}/mA · cm^{-2}	V_{oc}/mV	FF	η/%
QD_{566}	12.51	568	0.54	3.83
QD_{590}	14.84	555	0.57	4.68
QD_{615}	16.66	545	0.57	5.17
QD_{626}	18.02	527	0.56	5.32

The incidental photo-to-current efficiency (IPCE) spectra in Figure 6b further verified the generation of high photocurrent in the assembled cell devices. The IPCE spectra exhibit a strong photoresponse over the entire visible light range, with photon wavelengths covering 350−700 nm for the QD_{626}. It should be highlighted that the high IPCE value covered the whole photoresponse range and thus displays a nearly rectangle shape. This IPCE feature may derive from the intrinsic electronic characteristics of the inverted type-I core/shell structure sensitizer. It has been shown that, for the CdS/CdSe-sensitized electrode, the higher IPCE response in the short-wavelength region is due to the strong absorptivity of CdS in this spectral window, whereas CdSe harvests light efficiently in the long-wavelength region; together a better overall IPCE response was thus observed.[14,35−37] From the spectra we can find that a greater IPCE value and a wider response wavelength range are observed with the red-shift of the absorption onset of the QD sensitizers, which is consistent with the variation trend of J_{sc} values as observed in the $J-V$ measurement. IPCEs of ~85% between 400 and 650 nm were achieved with the QD_{626} sensitizer. Since the IPCE is found to be within a few percent of the transmission of the FTO substrate in this wavelength range, it could be concluded that light harvesting, charge separation, and charge collection are all close to unity when the CdS/CdSe

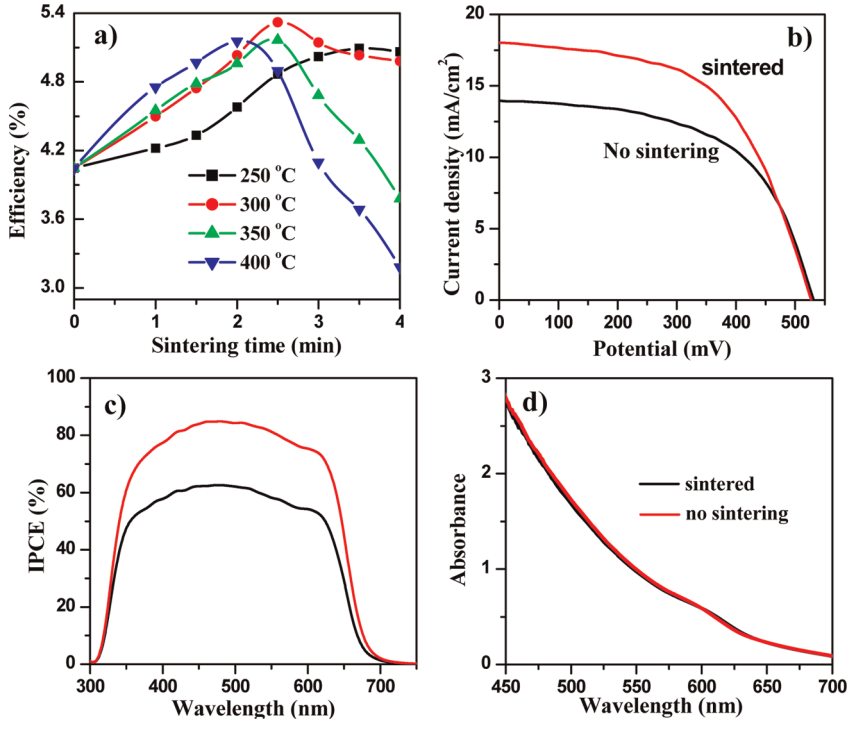

Figure 7. (a) Temporal evolution of conversion efficiencies of electrodes sintered at different temperatures. $J-V$ curves (b) and IPCE spectra (c) of QD_{626}-sensitized solar cells with and without sintering treatment, respectively. (d) Adsorption spectra of QD_{626}-sensitized TiO_2 electrodes with and without sintering treatment.

TABLE 2. Photovoltaic Characteristics of QDSCs before and after Sintering Treatment

	J_{sc}/mA·cm^{-2}	V_{oc}/mV	FF	η/%
after sintering	18.02	527	0.56	5.32
without sintering	13.97	531	0.56	4.15

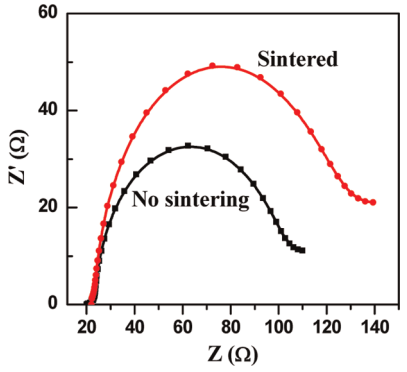

Figure 8. Experimental EIS spectra of QDSCs before and after sintering treatment of TiO_2 photoelectrodes. The corresponding fits (continuous lines) are also shown.

core/shell-sensitized electrodes are used. By integrating the product of the incident photon flux density and the cell's IPCE spectra, J_{sc} can then be calculated.[56] The calculated J_{sc} for the case of QD_{626} is 15.74 mA·cm^{-2}, which is quite close to the measured value (18.02 mA·cm^{-2}).

Influence of Sintering Treatment on QDSC Performance. Ko and co-workers have found that sintering treatment of photoanodes can somehow enhance the performance of QDSCs, especially the J_{sc} value.[10,11,57] In their report,[11] the sintering treatment was carried out by heating photoanodes using a hot-wind gun. We modified this process and carried it out in a more controllable and reproducible way with use of a muffle furnace. In the sintering experiment, the QD_{626}-sensitized TiO_2 electrodes were put into a 10 L muffle-type furnace at a prestabilized temperature for a certain period of time and then took them out of the furnace and cooled them naturally to room temperature. The effects of sintering time and temperature were systematically investigated, and the results are illustrated in Figure 7a. Obviously, there is a profound influence of both the sintering temperature and sintering time on the conversion efficiencies of the final solar cell. Under all four sintering temperatures (250, 300, 350, and 400 °C), we can find that the η value increased systematically in the beginning stage of the sintering process; after approaching the maximum point the η decreased gradually with extended sintering time. The maximum value of η came sooner with the increase of sintering temperature (*i.e.*, 250 °C corresponding to 3.5 min, both 300 and 350 °C corresponding to 2.5 min, and 400 °C corresponding to 2 min). In addition, the rate of decrease of the η value is sharper at higher sintering temperatures in the oversintering stage. The highest η value of 5.32% can be obtained under a sintering temperature of 300 °C for 2.5 min. From the *J*–*V* curves in Figure 7b and the photovoltaic characteristics in Table 2, we can find that after sintering at 300 °C for 2.5 min, the J_{sc} value increased from 13.97 to 18.02 mA/cm^{-2}, the corresponding η values increased from 4.15% to 5.32%, while the V_{oc} values stayed almost constant. The IPCE spectra (Figure 7c) also show significant improvement of IPCE value after sintering treatment. In comparison with the ~60% IPCE value before sintering treatment, the maximal IPCE value can be improved to as high as 85% after sintering under optimized conditions. Considering the process of photocurrent generation, IPCE is the combined effect of light-harvesting efficiency, electron-injecting efficiency, and electron-collecting efficiency. The absorption spectra (Figure 7d) of the electrodes before and after sintering treatment almost coincide, which indicates that this sintering treatment has no particularly significant impact on the electronic properties of the QD sensitizer. So the IPCE results mainly rely on the electron-injecting efficiency in the case where other parameters remain constant. The remarkable improvement of the IPCE value after sintering once again proves that this treatment is extremely beneficial for attaining a better connection between QDs and TiO_2, thereby leading to higher electron-injecting efficiency. On the other hand, the presence of a linker molecule between the QDs and TiO_2 interface does not affect the band gap alignment. This can explain why the V_{oc} values remain constant before and after the sintering treatment. Two opposing effects exist in the sintering treatment. Simultaneously, sintering treatment would deteriorate the QD sensitizer via oxidization and aggregation effects. This could reduce the performance of the cell devices. Therefore, the performance of cell devices is dependent on the sintering treatment temperature and time. This can explain the observation that overextending the sintering time causes a decrease of conversion efficiency.

The deposition of previously prepared MPA-capped CdS/CdSe QDs onto a TiO_2 electrode was achieved *via* the bridge-linking effect of capping ligand MPA molecules around the QD's surface. Since the organic linker molecule MPA is an electric insulator, the presence of the linker molecule between the QD and the TiO_2 would produce an insulating barrier and thus diminish the electron-injection rate from QDs to TiO_2 substrate.[30] We can expect longer electron injection times for the linker molecule capped QDs connected to TiO_2 particulate film than for bare semiconductors directly connected to the oxide matrix.[30] So getting rid of the linker molecule between the QDs and TiO_2 by sintering treatment would enhance the contact between QDs and TiO_2 and then improve the electron

transfer rate and electron-injecting efficiency, accordingly increasing the J_{sc} and η values of the final cell devices. FTIR spectra of QD-bound TiO_2 electrodes before sintering treatment show the characteristic C−H stretching vibrations at 2800−3000 cm^{-1}, derived from the hydrocarbon chain portion of the MPA molecules, while the spectra of electrodes after sintering treatment show almost no signals in the C−H stretching vibration region (the corresponding IR spectra are shown in Figure S2). This clearly indicates the partial removal of the MPA linker molecule between the QDs and TiO_2 substrate by the sintering treatment procedure.

To further reveal the interfacial reactions of photoexcited electrons in the QDSCs with and without sintering treatment, electrochemistry impedance spectroscopy (EIS) analysis was performed. Figure 8 shows the electrochemical impedance spectra for the QD_{626}-sensitized solar cells with and without sintering treatment in the dark under a forward bias of −0.50 V with a frequency range of 0.1 Hz to 100 kHz. One semicircle was observed in the Nyquist plots for each cell (Figure 8). The semicircles in the Nyquist plots corresponding to a middle-frequency area (in the 10−100 Hz range) are attributed to the electron transfer at the TiO_2/QDs/electrolyte interface.[58,59] The radius of the semicircle corresponding to a sintered cell is larger than that without sintering treatment, indicating that the electron recombination resistance increases after sintering treatment. This further supports the hypothesis that sintering treatment can elicit a better connection between the QDs and TiO_2, leading to smoother electron transmission in the TiO_2 film, inhibiting the surface recombination of electrons at the electrode/electrolyte interface, and obtaining greater photocurrent in the cell devices.

CONCLUSIONS

Inverted type-I CdS/CdSe core/shell structure QD-sensitized solar cells exhibiting record η value of 5.32% (V_{oc} = 0.527 V, J_{sc} = 18.02 mA/cm^2, FF = 0.56) under full 1 sun illumination have been fabricated. Consistent with the high η and J_{sc} values, an IPCE value of up to 85% over almost the entire visible spectral region is observed. The organometallic high-temperature synthetic method ensures the access of well-defined, high-quality inverted type-I CdS/CdSe core/shell structure QD sensitizers, while the adoption of linker molecule MPA-capped water-soluble QDs renders a high loading amount of QD sensitizers onto TiO_2 film electrodes. The optimized sintering treatments (optimal sintering temperature and time) of QDs-sensitized TiO_2 photoanodes can partially remove linker molecules and enhance the contact between QD sensitizers and TiO_2 and thus improve the photovoltaic performance, especially the J_{sc} value, of the cell devices. The conversion efficiency of the CdS/CdSe-based QDSCs might be further improved with the use of CdS/CdSe QD sensitizers with longer absorption onsets *via* the modification of the synthetic method.

MATERIALS AND METHODS

Preparation of Oil-Soluble CdS/CdSe QDs. CdS core nanocrystals were first prepared *via* a modified literature method developed by our group.[47] Typically, 19.2 mg of CdO was dissolved in a solvent mixture containing 0.15 mL of oleic acid (OA) and 3.0 mL of octadecene (ODE) at 250 °C under N_2 flow. At this temperature, 1.0 mL of ODE-S (0.1 M) was injected into the reaction system, and the reaction mixture was stirred at 250 °C for 1 min. Subsequently, the system temperature was reduced to 200 °C for overgrowth of the CdSe shell. A 0.22 mL amount of the Se stock solution (0.4 M, prepared by dissolving selenium in trioctylphosphine) and 1.0 mL of OAm was added into the reaction vessel in sequence followed by addition of an equimolar amount of Cd precursor stock solution (prepared by dissolving CdO in OA and ODE (v/v, 1:1) at 250 °C) at a 20 min interval. When the optical spectra showed no further changes, another cycle of Se/Cd precursor solution was added repeatedly. The volume of the precursor stock solution added in each cycle should not exceed the amount needed for a whole monolayer (ML) of the CdSe shell. The amount was calculated from the respective volumes of concentric spherical shells with 0.35 nm thickness for 1 ML of CdSe. In the process of overcoating the CdSe shell around the CdS core, when the absorption onset wavelength of the resulting CdS/CdSe approached the desired value, the addition of the Cd/Se precursors was stopped and the reaction was terminated by lowering the reaction temperature to room temperature.

Preparation of MPA-Capped Water-Soluble CdS/CdSe QDs. The water solubilization of the as-prepared oil-soluble CdS/CdSe QDs was obtained by replacing the initial hydrophobic surfactants (OAm and/or OA) with mercaptopropionic acid according to a literature method.[60] Typically, MPA (0.212 g, 0.2 mmol) was dissolved in 0.3 mL of deionized water together with 1.0 mL of methanol, and the solution was then adjusted to pH 12 with 40% NaOH. The MPA−methanol solution was then added into 5.0 mL of CdS/CdSe QD chloroform solution (containing 0.2 mmol of CdS/CdSe) and stirred for 30 min to precipitate the QDs. Then 10.0 mL of water was added into the mixture, and stirring was continued for another 20 min. The solution was separated in two phases finally, the CdS/CdSe QDs were transferred into the superincumbent water from the underlying chloroform, the underlying organic phase was discarded, and the aqueous phase containing the QDs was collected. The free MPA ligand in the QD aqueous solution was isolated by precipitating the QDs with addition of acetone. The supernatant was discarded, and the pellet was then redissolved in water for use in the next step.

Fabrication of QD-Sensitized Photoelectrodes and Solar Cells. TiO_2 nanoparticulate electrodes were prepared by successively screen printing a 8 μm thick transparent layer (P25 paste) and a 4 μm thick light-scattering layer (200−400 nm TiO_2) over F:SnO_2-coated (FTO, 14 Ω/square) glass substrates, followed by sintering at 450 °C for 30 min in a muffle-type furnace. A post-treatment of the dried TiO_2 film with an aqueous solution of $TiCl_4$ (0.04 M) was then carried out according to typical procedures for dye cells. The obtained TiO_2 mesoporous films were then coated with QDs sensitizers.

For immobilization of QDs, 30 μL of a MAP-capped QDs aqueous solution (with absorbance of 2.0 at the first excitonic

absorption peak) was pipetted directly on the electrode surface and allowed to stay for 2 h before rinsing sequentially with water and ethanol and then drying with nitrogen. After the deposition was complete, the QD-absorbed TiO_2 film was coated with ZnS by twice dipping alternately into 0.1 M $Zn(OAc)_2$ and 0.1 M Na_2S solutions for 1 min/dip. After coating with the ZnS layer, the TiO_2 electrode was then subjected to sintering treatment in a muffle-type furnace in a temperature range of 200−400 °C for periods of time ranging from 0.5 to 5 min.

The cells were prepared by assembling the counter electrode and a QD-sensitized photoanode using a 50 μm thick scotch spacer and with a droplet (10 μL) of polysulfide electrolyte. The Cu_2S counter electrodes were prepared by immersing brass in a HCl solution at 70 °C for 5 min, and then the brass was vulcanized by injecting a polysulfide solution after the solar cell fabrication. The polysulfide electrolyte solution consists of 2.0 M Na_2S, 2.0 M S, and 0.2 M KCl in methanol−water (3:7, v/v) solution. For QDSCs prepared under each condition, three cells were prepared and tested in parallel, and the one with the medium value was chosen as the final data.

TEM Images and Optical Spectra. Transition electron microscopy images were obtained using a JEOL JEM-1400 instrument. The TiO_2 films with CdS/CdSe QD sensitizers (~4.0 μm thick without scattering layers) were scratched off the FTO glass and dispersed in ethanol with the help of ultrasonication, from which a few drops were taken over a TEM grid and dried for TEM images. The absorption spectra of CdS/CdSe QD-sensitized electrodes composed of ~4.0 μm thick TiO_2 films with dimensions of 2.0 × 1.0 cm (without scattering layers) were recorded on a UV−visible spectrophotometer (Shimadzu UV-2450).

Electrochemical and Photovoltaic Measurements. Electrochemical impedance spectroscopy measurements were conducted with an impedance analyzer (Zahner, Germany) at −0.5 V bias potential and 10 mV of amplitude over the frequency range of 0.1 Hz to 100 kHz under dark conditions. Photovoltaic measurements employed an AM 1.5 G solar simulator equipped with a 300 W xenon lamp (model no. 91160, Oriel). *I*−*V* curves were obtained by applying an external bias to the cell and measuring the generated photocurrent with a Keithley model 2400 digital source meter. The photoactive area was 0.237 cm^2. The IPCE was recorded on a Keithley 2000 multimeter under the illumination of a 150 W tungsten lamp with a monochromator (Spectral Product DK240).

Conflict of Interest: The authors declare no competing financial interest.

Acknowledgment. We thank the National Natural Science Foundation of China (No. 21175043), the Science and Technology Commission of Shanghai Municipality (11JC1403100, 10dz2220500), and the Fundamental Research Funds for the Central Universities for financial support.

Supporting Information Available: FTIR characterization of CdS/CdSe-bound TiO_2 electrode with and without sintering treatment at 300 °C for 2.5 min. This material is available free of charge *via* the Internet at http://pubs.acs.org.

REFERENCES AND NOTES

1. Barnham, K. W. J.; Mazzer, M.; Clive, B. Resolving the Energy Crisis: Nuclear or Photovoltaics? *Nat. Mater.* **2006**, *5*, 161–164.
2. Hodes, G. Comparison of Dye- and Semiconductor-Sensitized Porous Nanocrystalline Liquid Junction Solar Cells. *J. Phys. Chem. C* **2008**, *112*, 17778–17787.
3. Kamat, P. V. Quantum Dot Solar Cells. Semiconductor Nanocrystals as Light Harvesters. *J. Phys. Chem. C* **2008**, *112*, 18737–18753.
4. Kamat, P. V.; Tvrdy, K.; Baker, D. R.; Radich, J. G. Beyond Photovoltaics: Semiconductor Nanoarchitectures for Liquid-Junction Solar Cells. *Chem. Rev.* **2010**, *110*, 6664–6688.
5. Rühle, S.; Shalom, M.; Zaban, A. Quantum-Dot-Sensitized Solar Cells. *ChemPhysChem* **2010**, *11*, 2290–2304.
6. Nozik, A. J.; Beard, M. C.; Luther, J. M.; Law, M.; Ellingson, R. J.; Johnson, J. C. Semiconductor Quantum Dots and Quantum Dot Arrays and Applications of Multiple Exciton Generation to Third-Generation Photovoltaic Solar Cells. *Chem. Rev.* **2010**, *110*, 6873–6890.
7. Mora-Seró, I.; Bisquert, J. Breakthroughs in the Development of Semiconductor-Sensitized Solar Cells. *J. Phys. Chem. Lett.* **2010**, *1*, 3046–3052.
8. Tang, J.; Sargent, E. H. Infrared Colloidal Quantum Dots for Photovoltaics: Fundamentals and Recent Progress. *Adv. Mater.* **2011**, *23*, 12–29.
9. Yang, Z.; Chen, C.-Y.; Roy, P.; Chang, H.-T. Quantum Dot-Sensitized Solar Cells Incorporating Nanomaterials. *Chem. Commun.* **2011**, *47*, 9561–9571.
10. Fan, S.-Q.; Fang, B.; Kim, J. H.; Jeong, B.; Kim, C.; Yu, J.-S.; Ko, J. Ordered Multimodal Porous Carbon as Highly Efficient Counter Electrodes in Dye-Sensitized and Quantum-Dot Solar Cells. *Langmuir* **2010**, *26*, 13644–13649.
11. Fan, S.-Q.; Fang, B.; Kim, J. H.; Kim, J.-J.; Yu, J.-S.; Ko, J. Hierarchical Nanostructured Spherical Carbon with Hollow Core/Mesoporous Shell as a Highly Efficient Counter Electrode in CdSe Quantum-Dot-Sensitized Solar Cells. *Appl. Phys. Lett.* **2010**, *96*, 063501.
12. Yang, Z.; Chen, C.-Y.; Liu, C.-W.; Li, C.-L.; Chang, H.-T. Quantum Dot-Sensitized Solar Cells Featuring CuS/CoS Electrodes Provide 4.1% Efficiency. *Adv. Energy Mater.* **2011**, *1*, 259–264.
13. Radich, J. G.; Dwyer, R.; Kamat, P. V. Cu_2S Reduced Graphene Oxide Composite for High-Efficiency Quantum Dot Solar Cells. Overcoming the Redox Limitations of S_2^-/S_n^{2-} at the Counter Electrode. *J. Phys. Chem. Lett.* **2011**, *2*, 2453–2460.
14. Lee, Y.-L.; Lo, Y.-S. Highly Efficient Quantum-Dot-Sensitized Solar Cell Based on Co-Sensitization of CdS/CdSe. *Adv. Funct. Mater.* **2009**, *19*, 604–609.
15. Zhang, Q.; Guo, X.; Huang, X.; Huang, S.; Li, D.; Luo, Y.; Shen, Q.; Toyoda, T.; Meng, Q. Highly Efficient CdS/CdSe-Sensitized Solar Cells Controlled by the Structural Properties of Compact Porous TiO_2 Photoelectrodes. *Phys. Chem. Chem. Phys.* **2011**, *13*, 4659–4667.
16. Yu, X.; Liao, J.; Qiu, K.; Kuang, D.; Su, C. Dynamic Study of Highly Efficient CdS/CdSe Quantum Dot Sensitized Solar Cells Fabricated by Electrodeposition. *ACS Nano* **2011**, *5*, 9494–9500.
17. Im, S. H.; Lim, C.-S.; Chang, J. A.; Lee, Y. H.; Maiti, N.; Kim, H.-J.; Nazeeruddin, Md. K.; Grätzel, M.; Seok, S. I. Toward Interaction of Sensitizer and Functional Moieties in Hole-Transporting Materials for Efficient Semiconductor-Sensitized Solar Cells. *Nano Lett.* **2011**, *11*, 4789–4793.
18. Chang, J. A.; Rhee, J. H.; Im, S. H.; Lee, Y. H.; Kim, H.-J.; Seok, S. I.; Nazeeruddin, Md. K.; Grätzel, M. High-Performance Nanostructured Inorganic-Organic Heterojunction Solar Cells. *Nano Lett.* **2010**, *10*, 2609–2612.
19. Watson, D. F. Linker-Assisted Assembly and Interfacial Electron-Transfer Reactivity of Quantum Dot-Substrate Architectures. *J. Phys. Chem. Lett.* **2010**, *1*, 2299–2309.
20. Guijarro, N.; Lana-Villarreal, T.; Mora-Seró, I.; Bisquert, J.; Gómez, R. CdSe Quantum Dot-Sensitized TiO_2 Electrodes: Effect of Quantum Dot Coverage and Mode of Attachment. *J. Phys. Chem. C* **2009**, *113*, 4208–4214.
21. Sambur, J. B.; Riha, S. C.; Choi, D.; Parkinson, B. A. Influence of Surface Chemistry on the Binding and Electronic Coupling of CdSe Quantum Dots to Single Crystal TiO_2 Surface. *Langmuir* **2010**, *26*, 4839–4847.
22. Hyun, B.-R.; Zhong, Y.-W.; Bartnik, A. C.; Sun, L.; Abruña, H. D.; Wise, F. W.; Goodreau, J. D.; Matthews, J. R.; Leslie, T. M.; Borrelli, N. F. Electron Injection from Colloidal PbS Quantum Dots into Titanium Dioxide Nanoparticles. *ACS Nano* **2008**, *2*, 2206–2212.
23. Leventis, H. C.; O'Mahony, F.; Akhtar, J.; Afzaal, M.; O'Brien, P.; Haque, S. A. Transient Optical Studies of Interfacial Charge Transfer at Nanostructured Metal Oxide/PbS Quantum Dot/Organic Hole Conductor Heterojunctions. *J. Am. Chem. Soc.* **2010**, *132*, 2743–2750.
24. Zaban, A.; Mićić, O. I.; Gregg, B. A.; Nozik, A. J. Photosensitization of Nanoporous TiO_2 Electrodes with InP Quantum Dots. *Langmuir* **1998**, *14*, 3153–3156.

25. Peter, L. M.; Wijayantha, K. G. U.; Riley, D. J.; Waggett, J. P. Band-Edge Tuning in Self-Assembled Layers of Bi_2S_3 Nanoparticles Used To Photosensitize Nanocrystalline TiO_2. *J. Phys. Chem. B* **2003**, *107*, 8378–8381.
26. Bang, J. H.; Kamat, P. V. Quantum Dot Sensitized Solar Cells. A Tale of Two Semiconductor Nanocrystals: CdSe and CdTe. *ACS Nano* **2009**, *3*, 1467–1476.
27. Baker, D. R.; Kamat, P. V. Photosensitization of TiO_2 Nanostructures with CdS Quantum Dots: Particulate *versus* Tubular Support Architectures. *Adv. Funct. Mater.* **2009**, *19*, 805–811.
28. Sant, P. A.; Kamat, P. V. Interparticle Electron Transfer between Size-Quantized CdS and TiO_2 Semiconductor. *Phys. Chem. Chem. Phys.* **2002**, *4*, 198–203.
29. Sun, W.; Yu, Y.; Pan, H.; Gao, X.; Chen, Q.; Peng, L. CdS Quantum Dots Sensitized TiO_2 Nanotube-Array Photoelectrodes. *J. Am. Chem. Soc.* **2008**, *130*, 1124–1125.
30. Robel, I.; Subramanian, V.; Kuno, M.; Kamat, P. V. Quantum Dot Solar Cells. Harvesting Light Energy with CdSe Nanocrystals Molecularly Linked to Mesoscopic TiO_2 Films. *J. Am. Chem. Soc.* **2006**, *128*, 2385–2393.
31. Kongkanand, A.; Tvrdy, K.; Takechi, K.; Kuno, M.; Kamat, P. V. Quantum Dot Solar Cells. Tuning Photoresponse through Size and Shape Control of CdSe-TiO_2 Architecture. *J. Am. Chem. Soc.* **2008**, *130*, 4007–4015.
32. Chen, J.; Lei, W.; Deng, W. Q. Reduced Charge Recombination in a Co-Sensitized Quantum Qot Solar Cell with Two Different Sizes of CdSe Quantum Dot. *Nanoscale* **2011**, *3*, 674–677.
33. Mora-Seró, I.; Giménez, S.; Moehl, T.; Fabregat-Santiago, F.; Lana-Villareal, T.; Gómez, R.; Bisquert, J. Factors Determining the Photovoltaic Performance of a CdSe Quantum Dot Sensitized Solar Cell: the Role of the Linker Molecule and of the Counter Electrode. *Nanotechnology* **2008**, *19*, 424007.
34. Wang, H.; Luan, C.; Xu, X.; Kershaw, S. V.; Rogach, A. L. *In Situ versus ex Situ* Assembly of Aqueous-Based Thioacid Capped CdSe Nanocrystals within Mesoporous TiO_2 Films for Quantum Dot Sensitized Solar Cells. *J. Phys. Chem. C* **2012**, *116*, 484–489.
35. Ning, Z.; Tian, H.; Qin, H.; Zhang, Q.; Ågren, H.; Sun, L.; Fu, Y. Wave-Function Engineering of CdSe/CdS Core/Shell Quantum Dots for Enhanced Electron Transfer to a TiO_2 Substrate. *J. Phys. Chem. C* **2010**, *114*, 15184–15189.
36. Lee, Y.-L.; Huang, B.-M.; Chien, H.-T. Highly Efficient CdSe-Sensitized TiO_2 Photoelectrode for Quantum-Dot-Sensitized Solar Cell Applications. *Chem. Mater.* **2008**, *20*, 6903–6905.
37. Lee, H. J.; Bang, J.; Park, J.; Kim, S.; Park, S.-M. Multilayered Semiconductor (CdS/CdSe/ZnS)-Sensitized TiO_2 Mesoporous Solar Cells: All Prepared by Successive Ionic Layer Adsorption and Reaction Processes. *Chem. Mater.* **2010**, *22*, 5636–5643.
38. Yang, Z.; Chen, C.-Y.; Liu, C.-W.; Chang, H.-T. Electrocatalytic Sulfur Electrodes for CdS/CdSe Quantum Dot-Sensitized Solar Cells. *Chem. Commun.* **2010**, *46*, 5485–5487.
39. Sudhagar, P.; Jung, J. H.; Park, S.; Lee, Y.-G.; Sathyamoorthy, R.; Kang, Y. S.; Ahn, H. The Performance of Coupled (CdS: CdSe) Quantum Dot-Sensitized TiO_2 Nanofibrous Solar Cells. *Electrochem. Commun.* **2009**, *11*, 2220–2224.
40. Hossain, M. A.; Jennings, J. R.; Koh, Z. Y.; Wang, Q. Carrier Generation and Collection in CdS/CdSe-Sensitized SnO_2 Solar Cells Exhibiting Unprecedented Photocurrent Densities. *ACS Nano* **2011**, *5*, 3172–3181.
41. Zhu, G.; Pan, L.; Xu, T.; Sun, Z. CdS/CdSe-Cosensitized TiO_2 Photoanode for Quantum-Dot- Sensitized Solar Cells by a Microwave-Assisted Chemical Bath Deposition Method. *ACS Appl. Mater. Interfaces* **2011**, *3*, 3146–3151.
42. Zhong, X.; Xie, R.; Zhang, Y.; Basché, T.; Knoll, W. High-Quality Violet- to Red-Emitting ZnSe/CdSe Core/Shell Nanocrystals. *Chem. Mater.* **2005**, *17*, 4038–4042.
43. Balet, L. P.; Ivanov, S. A.; Piryatinski, A.; Achermann, M.; Klimov, V. I. Inverted Core/Shell Nanocrystals Continuously Tunable between Type-I and Type-II Localization Regimes. *Nano Lett.* **2004**, *4*, 1485–1488.
44. Giménez, S.; Mora-Seró, I.; Macor, L.; Guijarro, N.; Lana-Villarreal, T.; Gómez, R.; Diguna, L. J.; Shen, Q.; Toyoda, T.; Bisquert, J. Improving the Performance of Colloidal Quantum-Dot-Sensitized Solar Cells. *Nanotechnology* **2009**, *20*, 295204.
45. Lee, H. J.; Yum, J.-H.; Leventis, H. C.; Zakeeruddin, S. M.; Haque, S. A.; Chen, P.; Seok, S. I.; Grätzel, M.; Nazeeruddin, Md. K. CdSe Quantum Dot-Sensitized Solar Cells Exceeding Efficiency 1% at Full-Sun Intensity. *J. Phys. Chem. C* **2008**, *112*, 11600–11608.
46. Ning, Z.; Tian, H.; Yuan, C.; Fu, Y.; Qin, H.; Sun, L.; Ågren, H. Solar Cells Sensitized with Type-II ZnSe-CdS Core/Shell Colloidal Quantum Dots. *Chem. Commun.* **2010**, *47*, 1536–1538.
47. Zhong, X.; Feng, Y.; Zhang, Y. Facile and Reproducible Synthesis of Red-Emitting CdSe Nanocrystals in Amine with Long-Term Fixation of Particles Size and Size Distribution. *J. Phys. Chem. C* **2007**, *111*, 526–531.
48. Battaglia, D.; Li, J. J.; Wang, Y.; Peng, X. Colloidal Two-Dimensional Systems: CdSe Quantum Shells and Wells. *Angew. Chem., Int. Ed.* **2003**, *42*, 5035–5039.
49. Fabregat-Santiago, F.; Garcia-Belmonte, G.; Mora-Seró, I.; Bisquert, J. Characterization of Nanostructured Hybrid and Organic Solar Cells by Impedance Spectroscopy. *Phys. Chem. Chem. Phys.* **2011**, *13*, 9083–9118.
50. Mora-Seró, I.; Giménez, S.; Fabregat-Santiago, F.; Gómez, R.; Shen, Q.; Toyoda, T.; Bisquert, J. Recombination in Quantum Dot Sensitized Solar Cells. *Acc. Chem. Res.* **2009**, *42*, 1848–1857.
51. Fang, Z.; Liu, L.; Wang, J.; Zhong, X. Depositing a $Zn_xCd_{1-x}S$ Shell around CdSe Core Nanocrystals *via* a Noninjection Approach. *J. Phys. Chem. C* **2009**, *113*, 4301–4306.
52. Hagfeldt, A.; Boschloo, G.; Sun, L.; Kloo, L.; Pettersson, H. Dye-Sensitized Solar Cells. *Chem. Rev.* **2010**, *110*, 6595–6663.
53. Lee, W.; Kang, S. H.; Min, S. K.; Sung, Y.-E.; Han, S.-H. Co-Sensitization of Vertically Aligned TiO_2 Nanotubes with Two Different Sizes of CdSe Quantum Dots for Broad Spectrum. *Electrochem. Commun.* **2008**, *10*, 1579–1582.
54. Leschkies, K. S.; Divakar, R.; Basu, J.; Enache-Pommer, E.; Boercker, J. E.; Carter, C. B.; Kortshagen, U. R.; Norris, D. J.; Aydil, E. S. Photosensitization of ZnO Nanowires with CdSe Quantum Dots for Photovoltaic Devices. *Nano Lett.* **2007**, *7*, 1793–1798.
55. Chen, J.; Zhao, D. W.; Song, J. L.; Sun, X. W.; Deng, W. Q.; Liu, X. W.; Lei, W. Directly Assembled CdSe Quantum Dots on TiO_2 in Aqueous Solution by Adjusting pH Value for Quantum Dot Sensitized Solar Cells. *Electrochem. Commun.* **2009**, *11*, 2265–2267.
56. Tachibana, Y.; Hara, K.; Sayama, K.; Arakawa, H. Quantitative Analysis of Light-Harvesting Efficiency and Electron-Transfer Yield in Ruthenium-Dye-Sensitized Nanocrystalline TiO_2 Solar Cells. *Chem. Mater.* **2002**, *14*, 2527–2535.
57. Fan, S.-Q.; Kim, D.; Kim, J.-J.; Jung, D. W.; Kang, S. O.; Ko, J. Highly Efficient CdSe Quantum-Dot-Sensitized TiO_2 Photoelectrodes for Solar Cell Applications. *Electrochem. Commun.* **2009**, *11*, 1337–1339.
58. González-Pedro, V.; Xu, X.; Mora-Seró, I.; Bisquert, J. Modeling High-Efficiency Quantum Dot Sensitized Solar Cells. *ACS Nano* **2010**, *4*, 5783–5790.
59. Kern, R.; Sastrawan, R.; Ferber, J.; Stangl, R.; Luther, J. Modeling and Interpretation of Electrical Impedance Spectra of Dye Solar Cells Operated under Open-Circuit Conditions. *Electrochim. Acta* **2002**, *47*, 4213–4225.
60. Liu, L.; Guo, X.; Li, Y.; Zhong, X. Bifunctional Multidentate Ligand Modified Highly Stable Water-Soluble Quantum Dots. *Inorg. Chem.* **2010**, *49*, 3768–3775.